Protein dynamics and stability: The distribution of atomic fluctuations in thermophilic and mesophilic dihydrofolate reductase derived using elastic incoherent neutron scattering

Lars Meinhold[a,b,*], David Clement[c,d], Moeava Tehei[c,d], Roy Daniel[c], John L. Finney[e], and Jeremy C. Smith[a,f]

[a] Heidelberg University, Interdisciplinary Center for Scientific Computing (IWR), Computational Molecular Biophysics, Im Neuenheimer Feld 368, 69120 Heidelberg, Germany.

[b] present address: California Institute of Technology, Physical Biology Center for Ultrafast Science and Technology, 1200 East California Boulevard, Pasadena, CA 91125, USA.

[c] Department of Biological Sciences, University of Waikato, Private Bag 3105, Hamilton, New Zealand.

[d] Institut Laue-Langevin, 6 Rue Jules Horowitz, BP 156, 38042 Grenoble Cedex 9, France.

[e] Department of Physics and Astronomy, University College London, London WC1E 6BT, Great Britain.

[f] University of Tennessee/Oak Ridge National Laboratory Center for Molecular Biophysics, Oak Ridge National Laboratory, P.O. Box 2008, Oak Ridge, TN 37831-6164, USA.

[*] email: lars.meinhold@caltech.edu

(dated: January 18, 2008)

ABSTRACT

The temperature dependence of the dynamics of mesophilic and thermophilic dihydrofolate reductase is examined using elastic incoherent neutron scattering. It is demonstrated that the distribution of atomic displacement amplitudes can be derived from the elastic scattering data by assuming a (Weibull) functional form that resembles distributions seen in molecular dynamics simulations. The thermophilic enzyme has a significantly broader distribution than its mesophilic counterpart. Furthermore, although the rate of increase with temperature of the atomic mean-square-displacements extracted from the dynamic structure factor is found to be comparable for both enzymes, the amplitudes are found to be slightly larger for the thermophilic enzyme. Therefore, these results imply that the thermophilic enzyme is the more flexible of the two.

Introduction

Protein function is commonly understood to depend both on the three-dimensional structure and the dynamics of the polypeptide chain. Further, it has been proposed that increased structural stability of proteins arises from increased rigidity, while increased flexibility may favour higher activity [1–3].

Proteins extracted from mesophilic and thermophilic organisms are interesting subjects for studying the relationships between protein structural stability, dynamics and function [4, 5]. A structural comparison between mesophilic and thermophilic protein homologs has revealed that different protein families employ different structural mechanisms to adapt to higher temperatures, with the only systematic rule being an increase in the number of ion pairs with increasing growth temperature [6]. This suggests that dynamics may play an important role in thermal stability.

Thermophilic enzymes, which are stable and catalytically active at higher temperatures than their mesophilic counterparts, have therefore been hypothesised to have higher rigidity and correspondingly lower activity than their mesophilic counterparts [7–10]. According to this 'corresponding state' hypothesis, at moderate temperature the thermophilic protein is less flexible than its mesophilic counterpart but both proteins exhibit the same flexibility when compared at their respective optimal growth temperature. However, some questions have been raised regarding the inverse relationship between activity and stability, as mediated by dynamics [2]. For example, and in contrast to the above mentioned studies, a higher structural flexibility on the picosecond timescale has been measured for a thermostable α-amylase as compared with its mesophilic counterpart [11, 12]. Moreover, a study at moderate temperature of the millisecond-timescale flexibility of rubredoxin from a hyperthermophile organism has provided no evidence that enhanced conformational rigidity underlies thermal stability [13]. These seemingly contrasting findings underline the question raised above whether indeed dynamics plays a key role in the thermal adaptation of proteins, and whether this dynamics may be timescale dependent.

The protein studied here, dihydrofolate reductase (DHFR), is an enzyme important for cell growth. The structure and function of DHFR are well characterised, and DHFR from *Escherichia coli* (*Ec*) has become an important model for investigating the relationship between protein dynamics and catalytic function [14]. Here, the dynamics of DHFR extracted from mesophilic *Ec* and from thermophilic *Geobacillus stearothermophilius* (*Bs*) are studied over a physiological temperature range (of *Ec*) on the sub-nanosecond timescale. Although motions on this timescale do not comprise the full range required for enzymatic function they are indicative of global flexibility. DHFR from *Ec* and *Bs* show closely similar overall and secondary structures as is shown in Fig. 1a,b [15, 16]. However, the X-ray crystallographic B (or temperature) factors, which are indicative of equilibrium structural flexibility, and are shown in Fig. 1c, suggest that *Bs*DHFR is, on average, more flexible than its mesophilic *Ec* counterpart.

The pico- to nanosecond timescale dynamics present in proteins can be determined using incoherent neutron scattering (INS) [17]. INS has been extensively used to study the dynamics of proteins and, in particular, to characterise the temperature-dependent change in inferred dynamics that is often referred to as the dynamical transition [18]. Much of the dynamical transition work has involved the examination of the elastic incoherent neutron scattering (EINS) from which the average atomic mean-square displacements (MSD) can be derived [19]. The physical models used to interpret the experimental EINS data have been extensively tested using molecular dynamics simulations. It has been shown that dynamical inhomogeneity in a protein contributes significantly to EINS [20–22]. Furthermore, diffusive protein motions and the finite energy resolution of the spectrometer also influence EINS [23–25]. However, a method

still commonly-used to extract atomic fluctuations from experimental EINS data assumes that all atoms have the same, *i.e.*, an average, fluctuation amplitude. In order to avoid using this oversimplified description, in the present report a model based on a distribution function for the atomic fluctuations is proposed and used to analyse the experimental EINS data.

Methods

Sample Preparation

Chemicals: Deuterium oxide (D_2O, 99.9% and 98%) was purchased from Minipul, Norell Inc. (Landisville, NJ., USA). Reagents and medium components for the purification and the analysis of variant DHFRs were purchased from Sigma-Aldrich Inc. (St.Louis, MO., USA) and Merck KgaA (Darmstadt, Germany).

Overexpression and purification of recombinant *Ec* and *Bs*DHFR: Recombinant variants of *Ec*DHFR (provided by Carston R Wagner, University of Minnesota) and *Bs*DHFR (provided by Judith Klinman, University of California at Berkeley) were purified from *Ec* cells (BL21 (DE3)) bearing the plasmid encoding for the DHFR genes, pTZwt1-3 and pET-21a respectively. The *Ec*DHFR variant was purified by a one step procedure [26], using methotrexate affinity chromatography (Sigma). The *Bs*DHFR enzyme was first partially purified by heat denaturation (incubation 20 min at 55°C) and then subjected to anion exchange chromatography instead of affinity chromatography [27]. Afterwards, a final ultrafiltration step (Amicon concentrator, YM-10 membrane) was carried out. Finally, the enzymes were lyophilised and kept at 4°C. Their purity was assessed by SDS gel electrophoresis.

Neutron scattering sample preparation: The purified protein was dissolved in D_2O (purity 98%) and gently stirred at room temperature overnight to replace the labile hydrogen atoms by deuterium and then freeze dried. The operation was repeated two more times with higher grade D_2O (purity 99.9%) and the sample was then freeze dried and stored at 4°C until use. The dry enzyme (115mg) was mixed into D_2O (345mg) as a homogenous highly-concentrated solution (300mg protein/ml) in which protein translational and rotational diffusion is likely to be considerably lower than in a dilute solution. The samples were then sealed in a flat aluminium sample holder (dimension 0.4x30x50 mm^3).

Neutron Scattering, Data Acquisition and Processing

The neutron scattering experiments were performed on the IN13 backscattering spectrometer of the Institut Laue-Langevin (ILL) in Grenoble, France. This spectrometer is sensitive to the q-range $0.3\,\text{Å}^{-1} \leq q \leq 5.5\,\text{Å}^{-1}$, with an energy resolution of $8\mu eV$ corresponding to observable motions on the timescale of $40 - 100\,\text{ps}$ or faster.

Sample containers were mounted on a cryostat and cooled to $280\,\text{K}$ at a rate of $-5\,\text{Kmin}^{-1}$. Scattering data were taken at $280\,\text{K}$ and at intervals of $5\,\text{K}$ to $305\,\text{K}$ (heating rate $+5\,\text{Kmin}^{-1}$). At each temperature, the scattering intensity was integrated for four hours (280 and $285\,\text{K}$) or five hours (290 to $305\,\text{K}$) to ensure sufficient statistics. The weights of the sample containers were measured before and after the scattering experiment to ensure that no sample was lost during the experiment; no loss was detected.

The raw data were corrected for scattering of the empty sample container and pure solvent (D_2O), detector response (by using a standard vanadium sample), and for self-absorption events (by using the transmission of the sample) using the softwares `Capri` and `Elascan` provided by the ILL for IN13 to obtain $S_{\text{inc}}(q, 0; T)$ at various temperatures T.

Analysis of Neutron Scattering Data

INS provides information on the self-correlations of atomic motions [28]. Due to their large incoherent scattering cross-section, the scattering from hydrogens (^{1}H) dominates the EINS from the present samples. For a Gaussian scatterer the elastic incoherent scattering is given by [29]

$$S_{\text{inc}}(q, \omega = 0) = A \exp\left(-\frac{1}{6}\langle\Delta\mathbf{r}^2\rangle q^2\right), \tag{1}$$

where q is the momentum transfer of the scattered neutron, $\langle \triangle \mathbf{r}^2 \rangle(t) = \langle [\mathbf{R}(t) - \mathbf{R}(0)]^2 \rangle$ is the time-dependent mean-square displacement (MSD) of the scatterer on the timescale of the instrument, and A is a constant amplitude. Note that the time-dependent MSD is related to the static thermal atomic mean-square position fluctuation by $\langle u^2 \rangle = \frac{1}{2} \lim_{t \to \infty} \langle \triangle \mathbf{r}^2 \rangle(t)$.

In a commonly-used method to extract the temperature-dependent atomic MSD from $S_{\text{inc}}(q, 0)$, use is made of Eq. (1) and linear regressions are performed on $\log S_{\text{inc}}(q)$ plotted against q^2. However, as is shown in Fig. 2 the experimental $\log S_{\text{inc}}(q)$ data is not linear over the full q^2-range. This nonlinearity, which has also been reported in previous studies [18, 30–32], may, in principle, be due to anharmonic motion and/or the presence of dynamical inhomogeneity, *i.e.*, a distribution of MSD amplitudes. However, it has been demonstrated using molecular dynamics simulations that dynamic inhomogeneity is the major contributor [20, 22, 33, 34]. Furthermore, due to their large abundance in proteins, the (rotational) dynamics of methyl groups has recently been identified as contributing significantly to this dynamical inhomogeneity [32, 35–38].

Whereas Eq. (1) is not applicable for anharmonic motions, in the case of dynamical inhomogeneity and assuming that the scattering from individual atoms can be described by Eq. (1), the observed $S_{\text{inc}}(q, 0)$ is given by the sum

$$S_{\text{inc}}(q, 0; \{A_i, u_i\}) = \sum_{i=1}^{N_G} A_i \exp\left(-\frac{1}{6} \langle \triangle \mathbf{r}_i^2 \rangle q^2 \right), \tag{2}$$

where N_G is the number of distinct populations of Gaussian scatterers with MSD $\langle \triangle \mathbf{r}_i^2 \rangle$. A version of Eq. (2) has been used in Refs. [30, 31, 39] to perform independent linear regressions to distinct q-regions. For instance, in Ref. [39] the authors used Eq. (2) to fit experimental data taken from Ref. [18] with $N_G = 3$, but supplied the weights A_i. In doing so, the question arises of which number N_G should be used to yield a physically-meaningful description of the dynamics present while not over-fitting the data. Here, a generalisation of Eq. (2) is proposed by using the continuum limit,

$$S_{\text{inc}}(q, 0; A, \boldsymbol{\alpha}) = A \int_0^\infty d\langle \triangle \mathbf{r}^2 \rangle \, \rho\left(\langle \triangle \mathbf{r}^2 \rangle; \boldsymbol{\alpha} \right) \exp\left[-\frac{1}{6} \langle \triangle \mathbf{r}^2 \rangle q^2 \right], \tag{3}$$

where $\rho(\langle \triangle \mathbf{r}^2 \rangle; \boldsymbol{\alpha})$ is the distribution function of the MSD-amplitudes with a set of parameters $\boldsymbol{\alpha}$. In a recent molecular dynamics study it has been shown that the non-gaussian behaviour of the EISF of globular proteins can be well described using Eq. (3) [22].

A priori, the functional form of $\rho(\langle \triangle \mathbf{r}^2 \rangle)$ is not known. However, for a given system $\rho(\langle \triangle \mathbf{r}^2 \rangle)$ can be directly obtained from molecular dynamics simulation. In Fig. 3 $\rho(\langle \triangle \mathbf{r}^2 \rangle)$ is shown derived from an MD simulation of a globular protein [40]. $\rho(\langle \triangle \mathbf{r}^2 \rangle)$ strongly increases at small values of $\langle u \triangle \mathbf{r}^2 \rangle$, has a single maximum at $\langle \triangle \mathbf{r}^2 \rangle \approx 0.5 \, \text{Å}^2$ and then decreases with a tail to zero for larger $\langle \triangle \mathbf{r}^2 \rangle$. Besides this shape description, any analytical function for $\rho(\langle \triangle \mathbf{r}^2 \rangle; \boldsymbol{\alpha})$ must fulfil two other pre-requisites. First, since $\langle \triangle \mathbf{r}^2 \rangle < 0$ is unphysical $\rho(\langle \triangle \mathbf{r}^2 \rangle < 0) \equiv 0$, thus precluding the use of a Gaussian distribution. Second, the number of parameters $\boldsymbol{\alpha}$ should be small enough to allow meaningful fitting and interpretation. Here, a Weibull distribution was chosen as the functional form, given by [41]

$$\rho(\triangle \mathbf{r}; \alpha, \beta) = \frac{\alpha}{\beta} \left(\frac{\triangle \mathbf{r}}{\beta} \right)^{\alpha - 1} \exp\left[-\left(\frac{\triangle \mathbf{r}}{\beta} \right)^\alpha \right]. \tag{4}$$

The parameters α and β determine the shape and the scale of the distribution, respectively. As an example, a fit to the simulated MSD data is also shown in Fig. 3. Although the height of

the peak and the length of the tail in $\rho(\langle \triangle \mathbf{r}^2 \rangle)$ are underestimated by the Weibull distribution, the general shape is reproduced. Eqs. (3) and (4) were used to fit the experimental $S_{\mathrm{inc}}(q, 0)$ in a least-squares sense,

$$\min_{A,\alpha,\beta} \sum_{q} \left[S_{\mathrm{inc}}^{\mathrm{exp}}(q, 0) - S_{\mathrm{inc}}(q, 0; A, \alpha, \beta) \right]^2. \tag{5}$$

The average root-mean-square displacement (RMSD) $\mu_{\triangle \mathbf{r}} = \sqrt{\langle \triangle \mathbf{r}^2 \rangle}$ is then readily calculated from the distribution parameters [41],

$$\mu_{\triangle \mathbf{r}} = \beta \Gamma \left(1 + \frac{1}{\alpha} \right), \tag{6}$$

where $\Gamma(\cdot)$ denotes the Gamma function. To obtain an estimate of the error in $\mu_{\triangle \mathbf{r}}$ the fit was performed on 100 subsets of data points, randomly chosen from the full q-range with weights proportional to the inverse of their statistical error. Finally, note that for the limit $\alpha \to \infty$ the Weibull distribution Eq. (4) converges towards the Dirac distribution, such that the monodisperse Gaussian model is retrieved: With $\Gamma(1) = 1$ the limits for the mean and variance become $\lim_{\alpha \to \infty} \mu_{\triangle \mathbf{r}} = \beta \Gamma(1) = \beta$ and $\lim_{\alpha \to \infty} \sigma^2 = \lim_{\alpha \to \infty} \beta^2 \left[\Gamma \left(1 + \frac{2}{\alpha} \right) - \Gamma^2 \left(1 + \frac{1}{\alpha} \right) \right] = 0$, respectively. Vanishing variance and normalisation 1 are properties of the Dirac distribution, and it follows that $\lim_{\alpha \to \infty} \rho(\triangle \mathbf{r}; \alpha, \beta) = \delta(\triangle \mathbf{r} - \beta)$.

Results

In Fig. 2 are plotted $\log S_{\mathrm{inc}}(q,0)$ against q^2 for mesophilic and thermophilic DHFR at all temperatures studied (280–305 K) and over the full q-range. For comparison, for each enzyme the data are normalised such that for the lowest q-value $S_{inc}(q^2 = 0.038\,\text{Å}^{-2}, 0) = 1$ at all temperatures. With increasing temperature, the average slope in the scattering intensity increases for both samples, indicating an increase with temperature in the structural flexibility. The difference in scattering intensity from the Ec and Bs samples at all temperatures is plotted against q^2 in Fig. 2c. The figure shows a significant difference in low-q scattering ($q^2 \lesssim 6\,\text{Å}^{-2}$), whereas the differences at larger q are somewhat smaller. The inset to figure Fig. 2c shows that the integrated difference depends on temperature.

For both DHFR samples and all temperatures, $\log S_{\mathrm{inc}}(q,0)$ *vs.* q^2 clearly deviates from linearity (Fig. 2a,b), indicating the presence of anharmonic dynamics and/or dynamical inhomogeneity. Here, the analysis is performed assuming the validity of the Gaussian approximation but explicitly considering dynamical inhomogeneity, modelled by a Weibull distribution for the atomic displacements. The following analysis utilises only the elastic scattering data to study differences in the intramolecular flexibility between the two enzymes. In principle, translational and rotational diffusive whole-molecule motions are also present and will contribute to the elastic intensity in the back-scattering regime [19, 42]. However, the proteins Ec and BsDHFR have very similar mass (18.0 kDa and 18.7 kDa, respectively) and three-dimensional structure/shape (Fig. 1a,b), which determine the whole-molecule diffusive dynamics. Therefore, differences in the elastic scattering can, to a good approximation, be attributed to differences in the protein-internal dynamics.

A realistic description of the elastic scattering within the framework of the Gaussian approximation is given by Eq. (3). An example of the analysis of experimental data using the Weibull model, *i.e.* Eqs. (3–5), is presented in Fig. 4 and found to reproduce $S_{\mathrm{inc}}(q,0)$ reasonably well over the full q-range. In particular, the Weibull model provides an excellent fit to the data for $q^2 < 6\,\text{Å}^{-2}$, where $\log S_{\mathrm{inc}}(q,0)$ *vs.* q^2 is strongly nonlinear and the commonly-used analysis method using only Eq. (1) is inadequate.

Using Eqs. (3–5), the average RMS-displacements, $\mu_{\triangle\mathbf{r}}(T)$ were determined for both mesophilic Ec and thermophilic BsDHFR and are shown in Fig. 5. For both enzymes, $\mu_{\triangle\mathbf{r}}(T)$ significantly, and roughly linearly, increases with increasing temperature, with an approximately equal rate of increase. The BsDHFR data point at 305 K appears anomalous. If this point is not considered the slope of $\mu_{\triangle\mathbf{r}}(T)$ is the same for Ec and BsDHFR, being $0.036 \pm 0.005\,\text{Å}\,\text{K}^{-1}$ and $0.037 \pm 0.004\,\text{Å}\,\text{K}^{-1}$, respectively.

At a given temperature $\mu_{\triangle\mathbf{r}}(T)$ is somewhat larger for the thermophilic BsDHFR, implying that the thermophilic enzyme is more flexible than its mesophilic counterpart. However, $\mu_{\triangle\mathbf{r}}(T)$ provides only an average, *i.e.* an overall figure that relates to the protein flexibility. In the following, therefore, the utility of the Weibull model is demonstrated by directly visualising the estimated distributions of atomic fluctuation amplitudes.

In Fig. 6 are shown the temperature-dependent distributions, $\rho(\triangle\mathbf{r})$ of displacement amplitudes for both enzymes. The temperature dependence of $\rho(\triangle\mathbf{r})$ is similar for both enzymes. For both systems with increasing temperature the distribution $\rho(\triangle\mathbf{r})$ becomes broader and the maximum shifted to larger displacement amplitudes. However, this behaviour is significantly stronger for the thermophilic BsDHFR, for which the distribution $\rho_{\mathrm{Bs}}(\triangle\mathbf{r})$ is significantly broader than $\rho_{\mathrm{Ec}}(\triangle\mathbf{r})$. Furthermore the shift of the distribution maximum is larger for the thermophilic BsDHFR: the maxima for $\rho_{\mathrm{Bs}}(\triangle\mathbf{r})$ and $\rho_{\mathrm{Ec}}(\triangle\mathbf{r})$ are at 1.6 Å and 1.5 Å, respectively, at 280 K but 2.1 Å and 1.8 Å at 300 K.

Fig. 6 also shows the temperature dependence of the Weibull fit parameters α and β. The

shape parameter α is similar for both enzymes and decreases with increasing temperature for T< 300 K, indicating a longer tail in the distribution, ρ. The average RMSD, $\mu_{\Delta\mathbf{r}}$, is only slightly affected by the variation of α in this parameter range. However, $\mu_{\Delta\mathbf{r}}$ is directly proportional to the scale parameter β. β is significantly larger for the thermophilic enzyme, indicating that ρ_{Bs} is broader than ρ_{Ec}. For both enzymes, β increases with increasing temperature. Thus, while the distributions of atomic fluctuations have approximately the same shape (determined by α) for both enzymes, the scale or width (determined by β) is larger for the thermophilic protein. With increasing temperature, the distributions for both enzymes become longer-tailed, reflecting that large-scale atomic fluctuations become more likely.

Discussion and Conclusion

The sub-nanosecond dynamics of mesophilic and thermophilic dihydrofolate reductase are studied here using elastic incoherent neutron scattering. The scattering data were analysed using a model based on the Gaussian approximation (quasi harmonic dynamics) that explicitly incorporates dynamical inhomogeneity using a distribution of atomic displacement amplitudes. Here, a Weibull function was used to model this distribution and the experimental scattering data were well reproduced over the full accessible q-range. In comparison, the commonly-used analysis method based on only one average fluctuation amplitude for all atoms, Eq. (1), typically needs to be restricted to certain q-ranges and, in particular, is incapable of reproducing $S_{\text{inc}}(q, 0)$ for the present samples at small q.

For mesophilic *Escherichia coli* DHFR the average RMS-displacements, $\mu_{\triangle\mathbf{r}}(T)$ increase from $1.6\,\text{Å}$ at $280\,\text{K}$ to $2.3\,\text{Å}$ at $305\,\text{K}$. Over the temperature range studied here, $\mu_{\triangle\mathbf{r}}(T)$ of *Ec*DHFR increases approximately linearly with temperature. For thermophilic *Geobacillus stearothermophilius* DHFR $\mu_{\triangle\mathbf{r}}(T)$ increases from $1.8\,\text{Å}$ at $280\,\text{K}$ to $2.6\,\text{Å}$ at $300\,\text{K}$. The decrease of $\mu_{\triangle\mathbf{r}}(T)$ in the last temperature step at $305\,\text{K}$ appears anomalous and may be erroneous. However, considering the relatively large uncertainty for the $300\,\text{K}$ $\mu_{\triangle\mathbf{r}}$-value a flattening of $\mu_{\triangle\mathbf{r}}(T)$ for $T \gtrsim 295\,\text{K}$ is also compatible with the experimental data.

A particular advantage of the present analysis method, *i.e.* the Weibull model, is that the distribution of atomic fluctuation amplitudes can be estimated. Although the Weibull model has only two adjustable parameters, the combination of a power law and an exponential function confers versatility on the distribution profile. Furthermore, a comparison between the results for $\mu_{\triangle\mathbf{r}}(T)$ and $\rho(T)$ in Figs. 5 and 6 shows that, due to the tail in the distribution ρ, $\mu_{\triangle\mathbf{r}}$ is generally larger than $\triangle\mathbf{r}_{\text{max}}$, *i.e.*, the position of the maximum in ρ. This also illustrates the difficulty of using only one single value (or moment) to characterise the distribution of atomic fluctuation amplitudes. For a strongly skewed ρ, the average fluctuation amplitude can be significantly different from the value where ρ is maximal. The ambiguity in distinguishing the contributions of protein-internal and whole-molecule dynamics to the elastic scattering remains but can, in principle, be alleviated by exploiting the quasielastic scattering [42]. This suggests an analysis method combining distribution functions for the amplitudes of internal fluctuations with rigid-body displacements for whole-molecule translation and rotation.

A further finding concerns the shape of the distribution of atomic displacement amplitudes. The present results indicate that this is broader for the thermophilic enzyme. The significance of this is that it suggests that a larger proportion of atoms in the thermophilic enzyme fluctuate with high amplitude. For example, in the distributions at $290\,\text{K}$ 17% of the atoms in the thermophilic enzyme fluctuate with $\triangle\mathbf{r} > 3.5\,\text{Å}$ whereas this value is 4% for the mesophilic species. One can speculate that this "highly-mobile fraction" might involve the relatively non-structured loops of the protein, thus preserving a relatively rigid functional core at higher temperatures. This hypothesis is supported by the observation that the offset between the $\mu_{\triangle\mathbf{r}}(T)$-slopes for *Ec*DHFR and *Bs*DHFR in Fig. 5 is $\approx 7\,\text{K}$, whereas their optimal growth temperatures differ by $\approx 15\,\text{K}$. Testing such hypotheses will become possible with specific deuteration and facilitated by the coming on line of next-generation neutron sources, such as the Spallation Neutron Source at Oak Ridge National Laboratory.

Finally, the biological relevance of the results for mesophilic and thermophilic protein dynamics is addressed. The importance of protein rigidity for structural stability has been discussed previously [1–3], but the question arises as to whether rigidity should refer to smaller displacements or a smaller change in displacements with increasing temperature. The present report finds the increase in flexibility with increasing temperature to be similar for both enzymes, whereas the fluctuation amplitudes are found to be slightly larger for the thermophilic enzyme. This suggests that thermophilic *Bs*DHFR is intrinsically more flexible than its mesophilic coun-

terpart *Ec*DHFR. The greater flexibility of the thermophilic enzyme may permit the larger fluctuation amplitudes at higher temperatures to be more easily accommodated within the native structure. Further studies on different proteins will be required to ascertain whether this is a general characteristic of mesophilic and thermophilic counterpart proteins.

References

[1] Daniel, R. M., 1986. *In* D. L. Oxender, editor, Protein Structure, Folding and Design, A R Liss, Inc., New York, volume 39 of *UCLA Symposia on Molecular and Cellular Biology, New Series*.

[2] Jaenicke, R., 2000. Do ultrastable proteins from hyperthermophiles have high or low conformational rigidity? *Proc Natl Acad Sci USA* 97:2926–2964.

[3] Arnold, F. H., P. L. Wintrode, K. Miyazaki, and A. Gershenson, 2001. How enzymes adapt: lessons from directed evolution. *Trends Biochem Sci* 26:100–106.

[4] Scandurra, R., V. Consalvi, R. Chiaraluce, L. Politi, and P. C. Engel, 1998. Protein thermostability in extremophiles. *Biochimie* 80:933–941.

[5] Fields, P. A., 2001. Review: Protein function at thermal extremes: balancing stability and flexibility. *Comp Biochem Phys A* 129:417–431.

[6] Szilagyi, A., and P. Zavodszky, 2000. Structural differences between mesophilic, moderately thermophilic and extremely thermophilic protein subunits: results of a comparative survey. *Structure* 8:493–504.

[7] Varley, P. G., and R. H. Pain, 1991. Relation between stability, dynamics and enzyme activity in 3-phosphoglycerate kinases from yeast and thermus thermophilus. *J Mol Biol* 220:531–538.

[8] Kohen, A., and J. P. Klinman, 2000. Protein flexibility correlates with degree of hydrogen tunneling in thermophilic and mesophilic alcohol dehydrogenases. *JACS* 122:10738–10739.

[9] Zavodszky, P., J. Kardos, A. Svingor, and G. A. Petsko, 1998. Adjustment of conformational flexibility is a key event in the the thermal adaptation of proteins. *Proc Natl Acad Sci USA* 95:7406–7411.

[10] Wolf-Watz, M., V. Thai, K. Henzler-Wildman, G. Hadjipavlou, E. Z. Eisenmesser, and D. Kern, 2004. Linkage between dynamics and catalysis in a thermophilic-mesophilic enzyme pair 11:945–949.

[11] Fitter, J., and J. Heberle, 2000. Structural equilibrium fluctuations in mesophilic and thermophilic α-amylase. *Biophys J* 79:1629–1636.

[12] Fitter, J., R. Herrmann, N. A. Dencher, A. Blume, and T. Hauss, 2001. Acticity and Stability of a thermostable α-amylase compared to its mesophilic homologue: mechanisms of thermal adaptation. *Biochemistry* 40:10723–10731.

[13] Hernandez, G., F. E. Jenney Jr, M. W. W. Adams, and D. M. LeMaster, 2000. Millisecond time scale conformational flexibility in a hyperthermophile protein at ambient temperature. *Proc Natl Acad Sci USA* 97:3166–3170.

[14] Schnell, J. R., H. J. Dyson, and P. E. Wright, 2004. Structure, dynamics, and catalytic function of dihydrofolate reductase. *Annu Rev Biophys Biomol Struct* 33:119–140.

[15] Kim, H. S., S. M. Damo, S. Y. Lee, D. Wemmer, and J. P. Klinman, 2005. Structure and hydride transfer mechanism of a moderate thermophilic dihydrofolate reductase from Bacillus stearothermophilus and comparison to its mesophilic and hyperthermophilic homologues. *Biochemistry* 44:11428–11439.

[16] Summerfield, R. L., D. M. Daigle, S. Mayer, D. Mallik, D. W. Hughes, S. G. Jackson, M. Sulek, M. G. Organ, E. D. Brown, and M. S. Junop, 2006. A 2.13Å Structure of E. coli Dihydrofolate Reductase Bound to a Novel Competitive Inhibitor Reveals a New Binding Surface Involving the M20 Loop Region. *J Med Chem* 49:6977–6986.

[17] Smith, J. C., 1991. Protein dynamics: comparison of simulations with inelastic neutron scattering experiments. *Quart Rev Biophys* 24:227–291.

[18] Doster, W., S. Cusack, and W. Petry, 1989. Dynamical transition of myoglobin revealed by inelastic neutron scattering. *Nature* 337:754–756.

[19] Gabel, F., D. Bicout, U. Lehnert, M. Tehei, M. Weik, and G. Zaccaï, 2002. Protein dynamics studied by neutron scattering. *Quart Rev Biophys* 35:327–367.

[20] Hayward, J. A., and J. C. Smith, 2002. Temperature Dependence of Protein Dynamics: Computer Simulation Analysis of Neutron Scattering Properties. *Biophys J* 82:1216–1225.

[21] Becker, T., J. A. Hayward, J. L. Finney, R. M. Daniel, and J. C. Smith, 2004. Neutron Frequency Windows and the Protein Dynamical Transition. *Biophys J* 87:1–9.

[22] Tokuhisa, A., Y. Joti, H. Nakagawa, A. K. A, and M. Kataoka, 2007. Non-Gaussian behavior of elastic incoherent neutron scattering profiles of proteins studied by molecular dynamics simulation. *Phys Rev E* 75:041912.

[23] Gabel, F., 2005. Protein dynamics in solution and powder measured by incoherent elastic neutron scattering: the influence of Q-range and energy resolution. *Eur Biophys J* 34:1–12.

[24] Gabel, F., and M. C. Bellissent-Funel, 2007. C-Phycocyanin Hydration Water Dynamics in the Presence of Trehalose: An Incoherent Elastic Neutron Scattering Study at Different Energy Resolutions. *Biophys J* 92:4054–4063.

[25] Kneller, G., 2007. Estimating the influence of finite instrumental resolution on elastic neutron scattering intensities from proteins. *J Chem Phys* 126:125107.

[26] Baccanari, D. P., D. Averett, C. Briggs, and J. Burchall, 1977. Escherichia coli dihydrofolate reductase: isolation and characterization of two isozymes. *Biochemistry* 16:3566–3572.

[27] Wilquet, V., J. A. Gaspar, M. van de Lande, M. V. de Casteele, C. Legrain, E. M. Meiering, and N. Glansdorff, 1998. Purification and characterization of recombinant Thermotoga maritima dihydrofolate reductase. *Eur J Biochem* 255:628–637.

[28] Bée, M., 1988. Quasielastic Neutron Scattering. Adam Hilger, Bristol and Philadelphia.

[29] van Hove, L., 1954. Correlations in space and time and Born approximation scattering in systems of interacting particles. *Phys Rev* 95:249–262.

[30] Réat, V., G. Zaccaï, M. Ferrand, and C. Pfister, 1997. Functional dynamics in purple membrane. *In* S. Cusack, H. Büttner, M. Ferrand, P. Langan, and P. Timmins, editors, Biological Macromolecular Dynamics, Adenine Press, Schenectady, New York.

[31] Lehnert, U., V. Réat, M. Weik, G. Zaccaï, and C. Pfister, 1998. Thermal Motions in Bacteriorhodopsin at Different Hydration Levels Studied by Neutron Scattering: Correlation with Kinetics and Light-Induced Conformational Changes. *Biophys J* 75:1945–1952.

[32] Doster, W., 2006. Dynamical structural distributions in proteins. *Physica B* 385-386:831–834.

[33] Becker, T., and J. C. Smith, 2003. Energy resolution and dynamical heterogeneity effects on elastic incoherent neutron scattering from molecular systems. *Phys Rev E* 67:021904.

[34] Hayward, J. A., J. L. Finney, R. M. Daniel, and J. C. Smith, 2003. Molecular Dynamics Decomposition of Temperature-Dependent Elastic Neutron Scattering by a Protein Solution. *Biophys J* 85:679–685.

[35] Curtis, J. E., M. Tarek, and D. J. Tobias, 2004. Methyl group dynamics as a probe of the protein dynamical transition. *JACS* 126:15928–15929.

[36] Doster, W., and M. Settles, 2005. Protein–water displacement distributions. *Biochim Biophys Acta* 1749:173–186.

[37] Roh, J. H., V. N. Novikov, R. B. Gregory, J. E. Curtis, Z. Chowdhuri, and A. P. Sokolov, 2005. Onsets of anharmonicity in protein dynamics. *Phys Rev Lett* 95:038101.

[38] Roh, J. H., J. E. Curtis, S. Azzam, V. N. Novikov, I. Peral, Z. Chowdhuri, R. B. Gregory, and A. P. Sokolov, 2006. Influence of hydration on the dynamics of lysozyme. *Biophys J* 91:2573–2588.

[39] Engler, N., A. Ostermann, N. Niimura, and F. G. Parak, 2003. Hydrogen atoms in proteins: Positions and dynamics. *Proc Natl Acad Sci USA* 100:10243–10248.

[40] Meinhold, L., and J. C. Smith, 2005. Fluctuations and Correlations in Crystalline Protein Dynamics: A Simulation Analysis of Staphylococcal Nuclease. *Biophys J* 88:2554–2563.

[41] Bronstein, I. N., K. A. Semendjajew, G. Musiol, and H. Mühlig, 1997. Taschenbuch der Mathematik. Verlag Harri Deutsch, Frankfurt am Main, Thun.

[42] Pérez, J., J. M. Zanotti, and D. Durand, 1999. Evolution of the Internal Dynamics of Two Globular Proteins from Dry Powder to Solution. *Biophys J* 77:454–469.

[43] Berman, H. M., J. Westbrook, Z. Feng, G. Gilliland, T. N. Bhat, H. Weissig, I. N. Shindyalov, and P. E. Bourne, 2000. The Protein Data Bank. *Nucleic Acids Res* 28:235–242.

Figure Captions

Figure 1: Structural comparison between mesophilic *Ec*DHFR (black/opaque) and thermophilic *Bs*DHFR (gray/transparent) in (**a**): cartoon and (**b**): space-filling van der Waals representation. In (**c**) the C_α-atom crystallographic B factors are plotted for both enzymes. The *Ec* and *Bs* structural coordinates and B factors were obtained from the Protein Data Bank [43] accession codes 2ANQ [16] and 1ZDR [15], respectively. Both structures were determined at the same temperature, $100\,\mathrm{K}$.

Figure 2: Elastic scattering intensity, $S_{\mathrm{inc}}(q,0)$ measured at various temperatures for (**a**): *Ec*DHFR and (**b**): *Bs*DHFR. For clarity, representative errorbars are shown only for the $280\,\mathrm{K}$ and $305\,\mathrm{K}$ data. Connecting lines are drawn for convenience and the vertical axes are logarithmic. In (**c**) is shown the difference, $\Delta_{\mathrm{Ec-Bs}}S_{\mathrm{inc}}(q,0) = S_{\mathrm{inc}}^{\mathrm{Ec}}(q,0) - S_{\mathrm{inc}}^{\mathrm{Bs}}(q,0)$, for each temperature; the inset shows the integrated difference, $\Sigma(T) = \Sigma_q \Delta_{\mathrm{Ec-Bs}}S_{\mathrm{inc}}(q,0)$ plotted against temperature, T.

Figure 3: Distribution of atomic mean-square displacements from a molecular dynamics simulation of crystalline Staphylococcal nuclease calculated from a $1\,\mathrm{ns}$ trajectory and with $\Delta t = 40\,\mathrm{ps}$ corresponding to the IN13 energy/time resolution. Simulation details are described elsewhere [40]. The simulation data is fitted using a Weibull distribution, Eq. (4), with the parameters $\alpha = 1.68$ and $\beta = 1.09$.

Figure 4: Example fit of the Weibull model, Eqs. (3–5), to the experimental elastic scattering data for thermophilic *Bs*DHFR at $300\,\mathrm{K}$ over the full q-range. The vertical axis is logarithmic.

Figure 5: Temperature dependence of the average RMS-displacements $\mu_{\Delta \mathbf{r}}$ obtained by fitting the Weibull model, Eqs. (3–5), to the experimental EISF data. Error bars denote the standard deviation for 100 fits to data subsets as described in the text. Lines connecting data points are drawn for convenience.

Figure 6: *Top:* Fit parameters α and β for the Weibull model plotted against temperature. *Bottom:* Average Weibull-distributions of RMS-displacements for mesophilic *Ec*DHFR and thermophilic *Bs*DHFR at $280\,\mathrm{K}$ (solid line), $290\,\mathrm{K}$ (dashed line) and $300\,\mathrm{K}$ (dotted line). For convenience, the profiles for *Bs*DHFR are vertically shifted by 0.4.
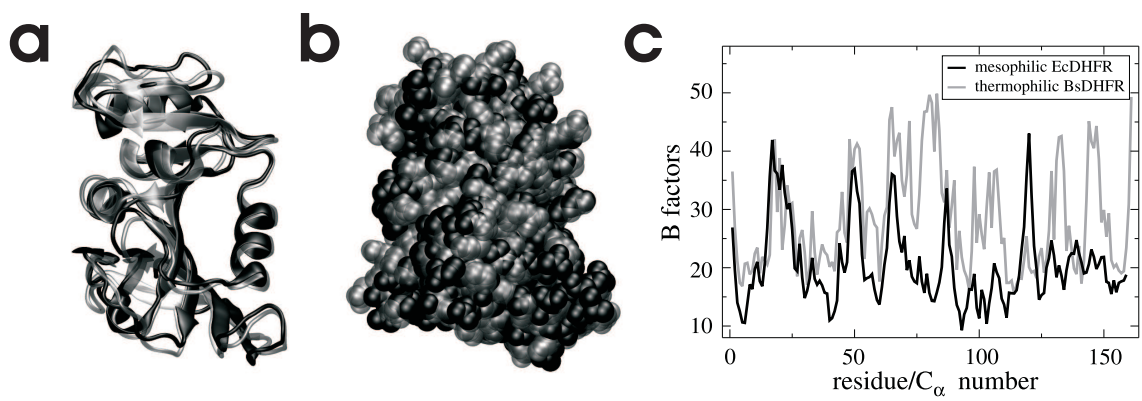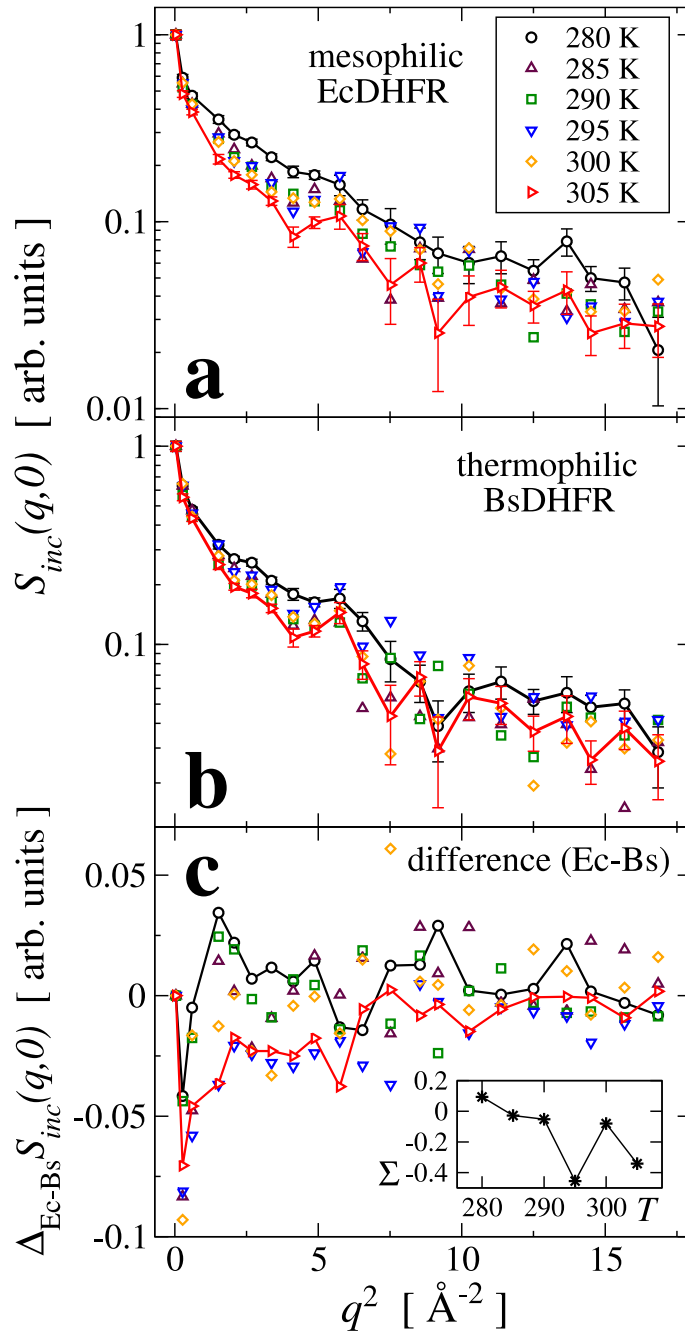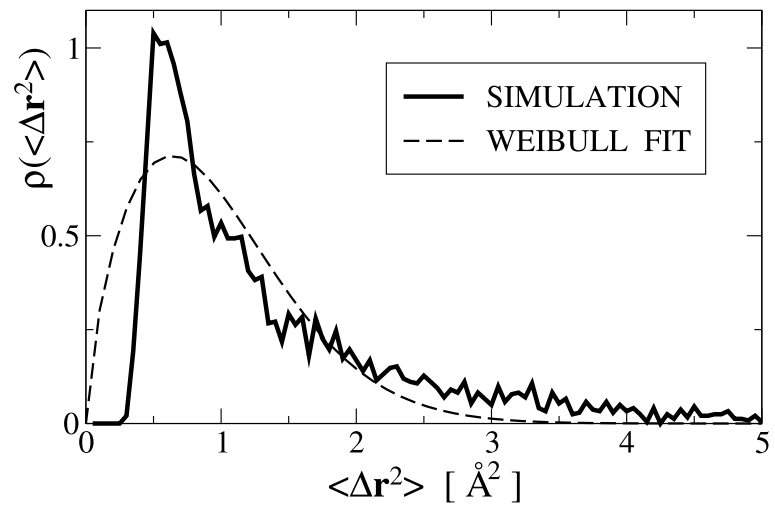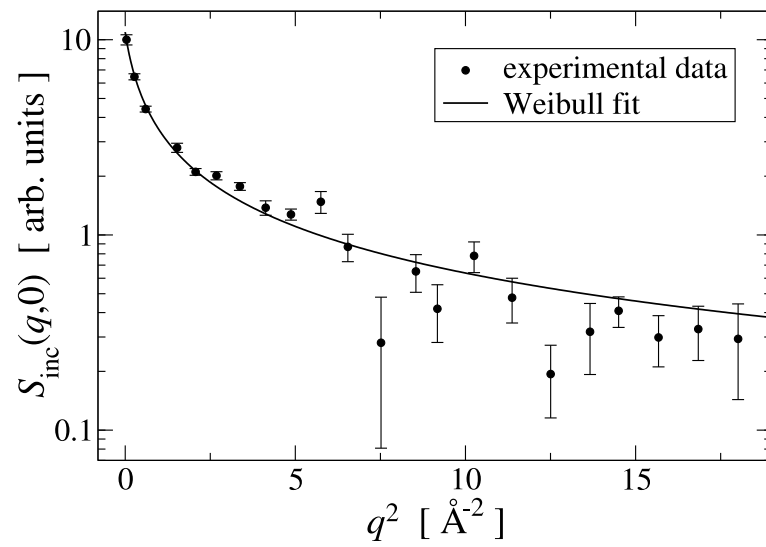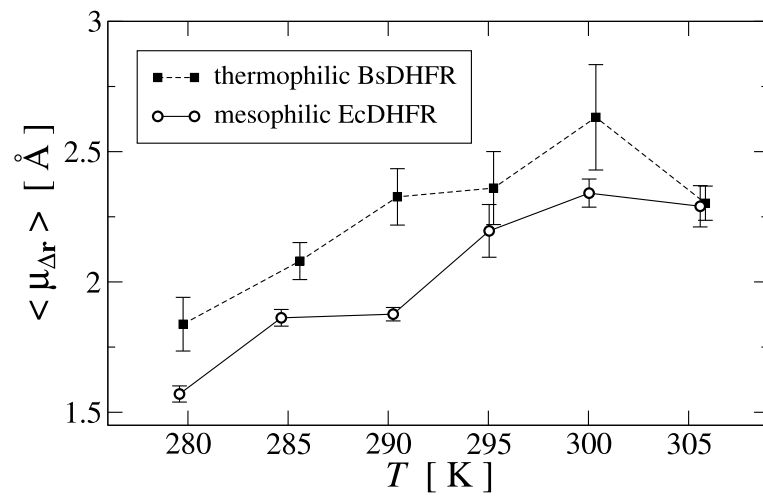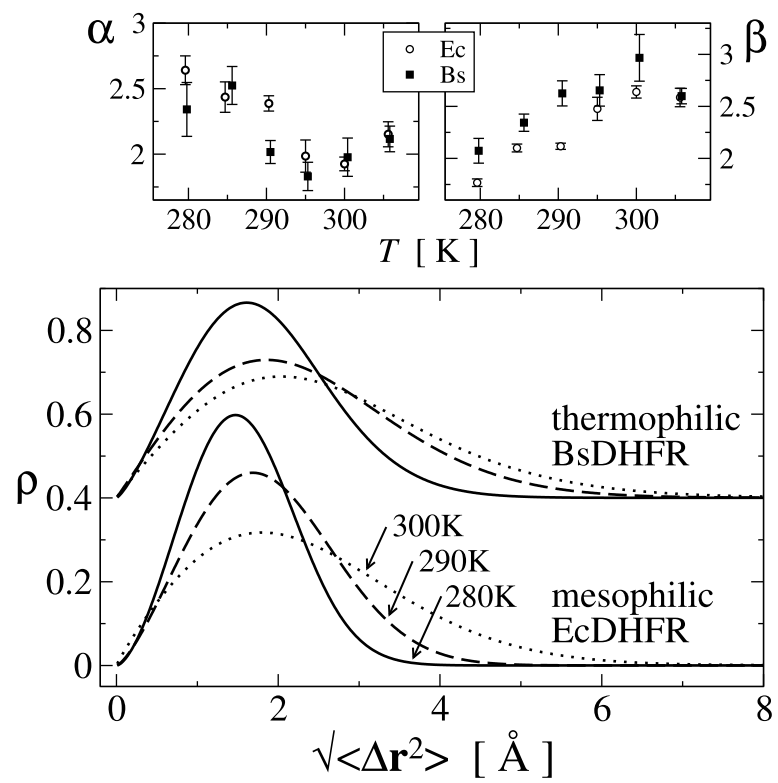
Figure 1:

Figure 2:

Figure 3:

Figure 4:

Figure 5:

Figure 6: